GSA Data Repository 2020008

Calcium isotope evidence for environmental variability before and across the Cretaceous – Paleogene mass extinction

Linzmeier et al.

This Data Repository entry contains:

- Supplementary Figures
  - Figure DR1 – All $\delta^{44/40}$Ca through section
  - Figure DR2 – Comparison of $\delta^{44/40}$Ca to $Wt\%_{carb}$ from ODP 690
  - Figure DR3 – Comparison of $\delta^{44/40}$Ca to elemental ratios
  - Figure DR4 – $\delta^{44/40}Ca_{SW}$ sensitivity to global change in $\Delta^{44/40}Ca_{carb\text{-}SW}$
- Supplementary Tables
  - Table DR1 – Sample list and museum information
  - Table DR2 – Seymour Island age model tie points
  - Table DR3 – Global age model tie points
  - Table DR4 – Trace element and $\delta^{44/40}$Ca dataset [*found in external Excel file*]
  - Table DR5 – $^{87}Sr/^{86}Sr$ dataset [*found in external Excel file*]
  - Table DR6 – Summary statistics of replicates
  - Table DR7 – Range of calcium concentrations for the Late Cretaceous
  - Table DR8 – Flux balance model parameters
- Supplementary Discussion
  - Extended description of geological setting
  - Extended analytical methods
  - Description of age model and correlation
  - Description of forward model
  - Discussion of calcium isotope fractionation and biomineralization
- Supplementary References

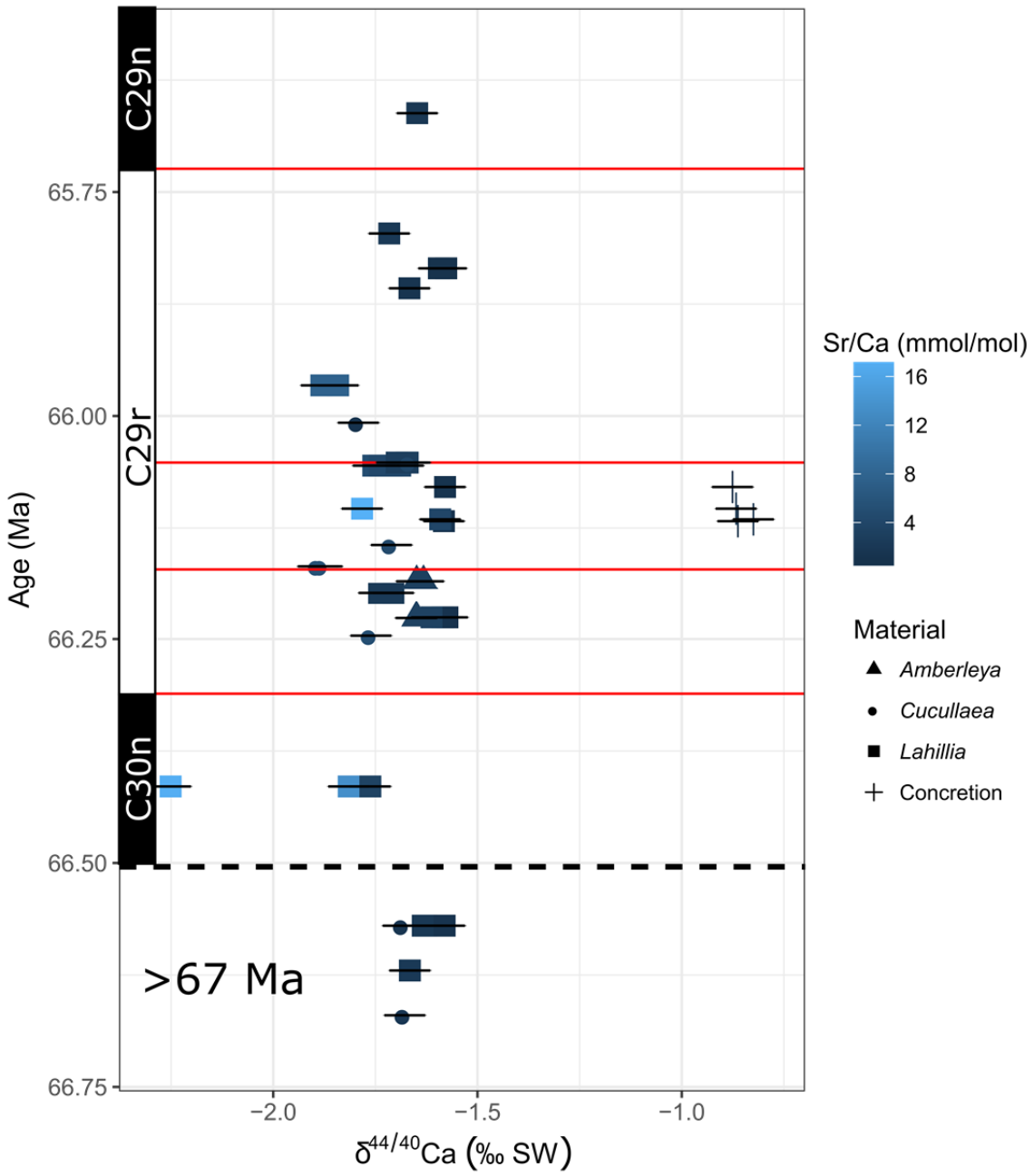

Data Repository Figure DR1. All $\delta^{44/40}$Ca through section

All analyses of $\delta^{44/40}$Ca through time at Seymour Island. Shells with high Sr/Ca and analyses of carbonate cement are excluded from Figure 3 in the main text. Note that shells with high Sr/Ca have lower $\delta^{44/40}$Ca compared to closely contemporaneous samples. Concretion carbonate cement has consistent $\delta^{44/40}$Ca near -0.8‰ across several samples, which may reflect the difference between biogenic aragonite and inorganic calcite (Blättler et al., 2012). The three red bars from bottom to top indicate the start of Deccan Traps volcanism, a putative local extinction, and the K-Pg extinction, respectively.

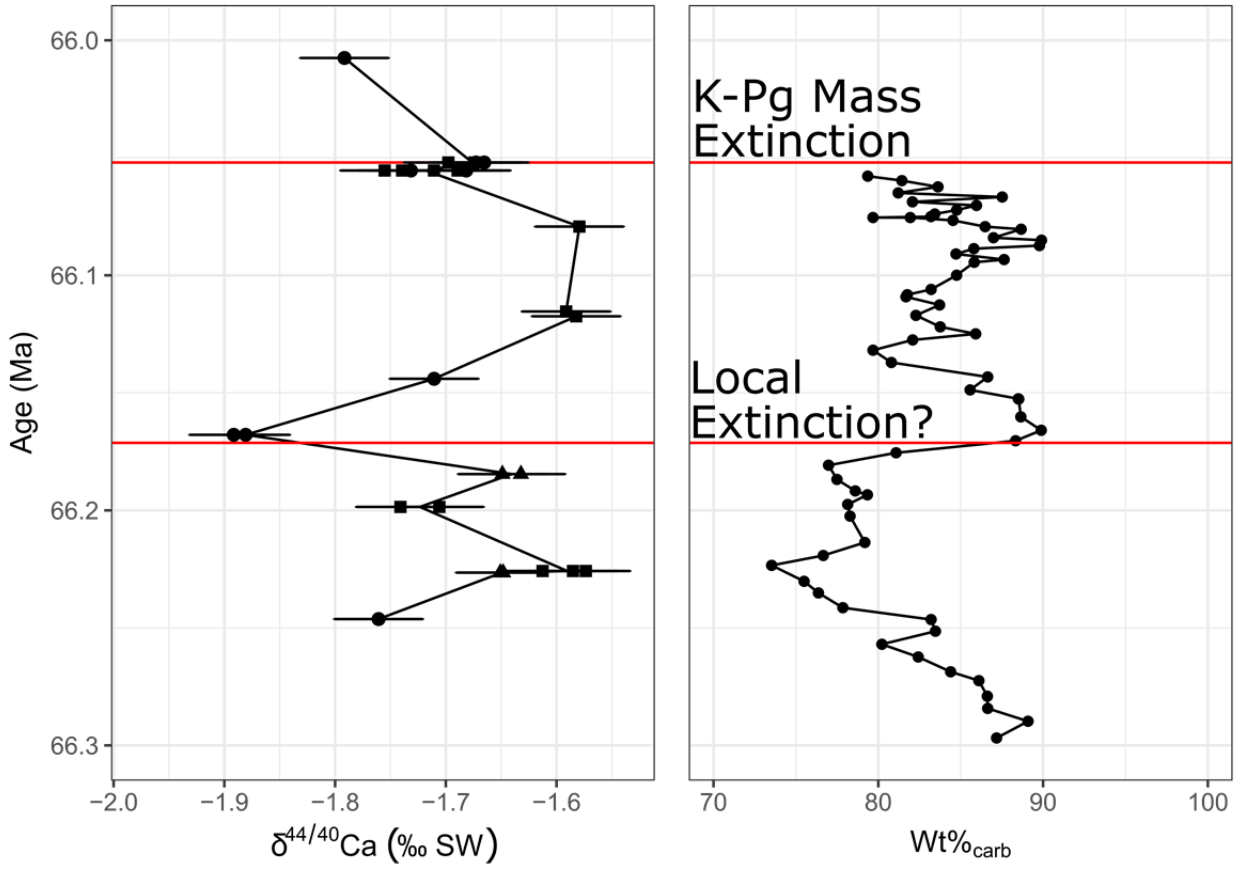

Data Repository Figure DR2. Comparison of $\delta^{44/40}$Ca to Wt%$_{carb}$ from ODP 690

Bivalve $\delta^{44/40}$Ca from low Sr/Ca samples near to the K-Pg boundary compared to variability in Wt%$_{carb}$ measured at ODP 690. Correlation based on the K-Pg boundary and 30N-29R reversal horizon with linear age interpolations between these horizons; see below for more specifics. The Wt%$_{carb}$ record from this site (Maud Rise) reflects both saturation state and carbonate production in the high latitude ocean (O'Connell, 1990; Ehrendorfer, 1993; Henehan et al., 2016). Modern high latitude oceans are likely more sensitive to saturation state change (Fabry et al., 2009). The slight decrease in Wt%$_{carb}$ below the K-Pg may be due to bioturbation (Henehan et al., 2016). Local minor extinction horizon from Tobin (2017).

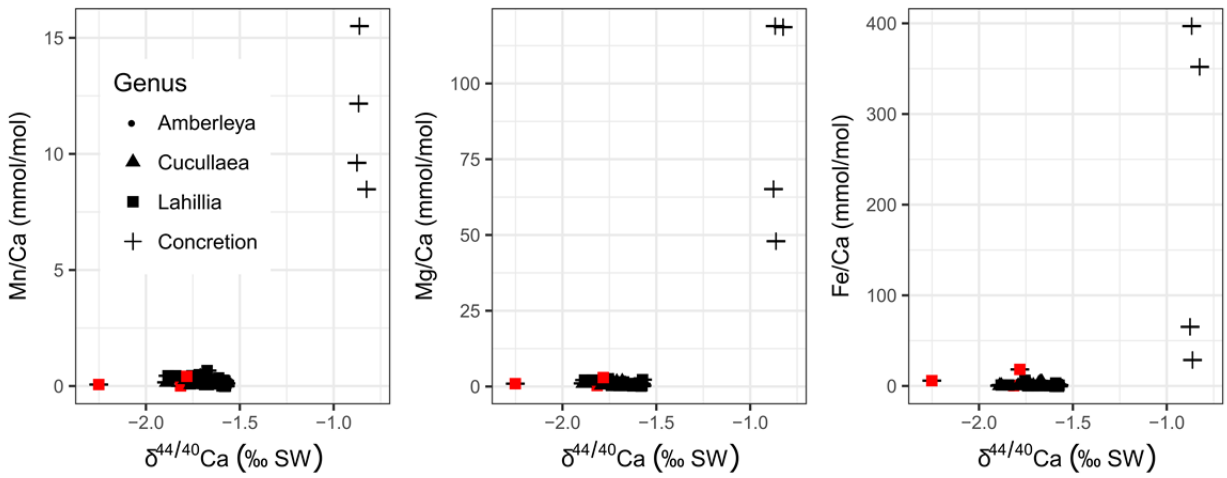

Data Repository Figure DR3. Comparison of $\delta^{44/40}$Ca to elemental ratios

All analyses of $\delta^{44/40}$Ca vs other elemental ratios measured by ICP-OES. Shells with Sr/Ca higher than 10 (mmol/mol) are highlighted in red. For most solutions the [Mn], [Mg], and [Fe] were below calibration range for solutions optimized for Ca and Sr concentrations. These data highlight the difference between shell material and concretion carbonate cement. The low Mn/Ca, Mg/Ca, and Fe/Ca also supports the preservation of unaltered shell.

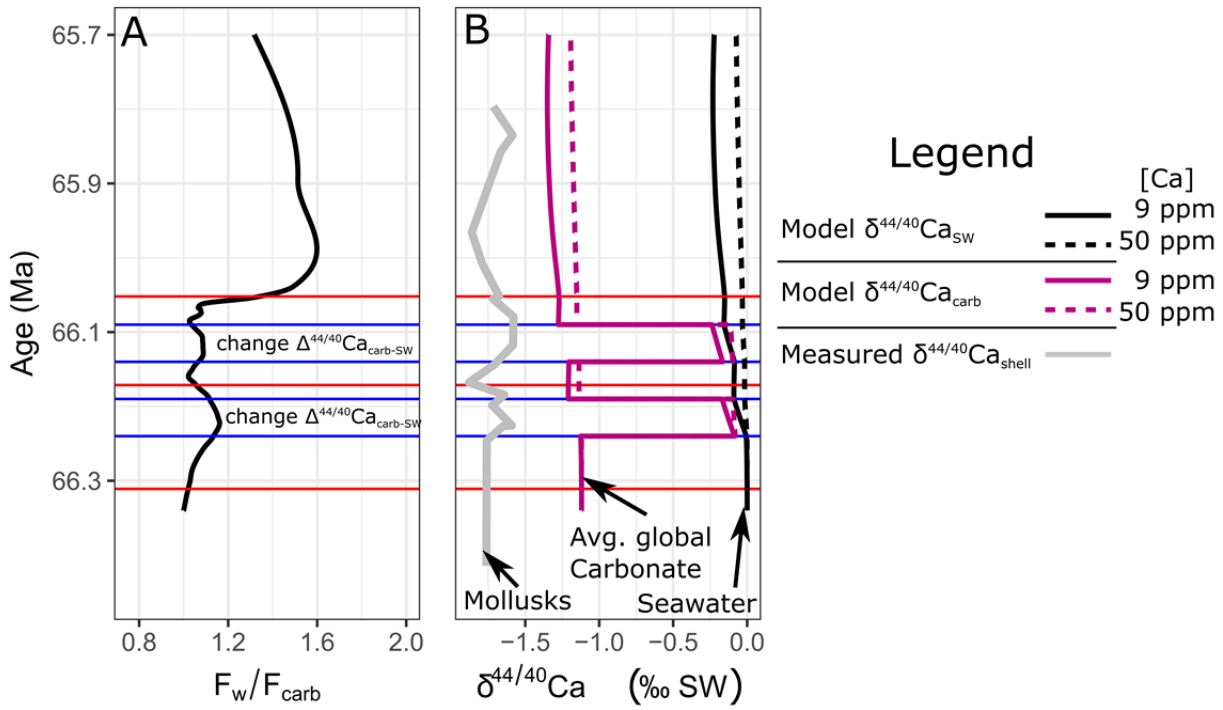

Data Repository Figure DR4. $\delta^{44/40}Ca_{SW}$ sensitivity to global change in both flux imbalance and $\Delta^{44/40}Ca_{carb\text{-}SW}$

A) Flux estimates are based on scaling the burial flux of carbonate (F_{carb}) using $Wt\%_{carb}$ at ODP 690 assuming constant weathering flux (F_w). The magnitude of the global carbonate fractionation factor ($\Delta^{44/40}Ca_{carb\text{-}SW}$) is reduced by 1.0‰ between the pairs of blue lines and then returns to the previous value (-1.12‰) outside of these lines. B) Modeled $\delta^{44/40}Ca_{SW}$ and $\delta^{44/40}Ca_{carb}$ at two [Ca] through time compared to the measured $\delta^{44/40}Ca_{shell}$. Even with large (~1.0‰) stepwise change to the global fractionation factor (between the blue lines), minimal $\delta^{44/40}Ca_{SW}$ change (<0.02‰) for the global ocean occurs over the timescale studied.

Data Repository Table DR1. Sample List and Museum Information

Sample	Museum*	Museum #	Class	Genus
C1174A.2	UM		Bivalvia	*Cucullaea*
C1184A2	UM		Bivalvia	*Cucullaea*
C1467A	UM		Bivalvia	*Cucullaea*
C1517A	UM		Bivalvia	*Cucullaea*
C1555B	UM		Bivalvia	*Cucullaea*
C477B	UM		Bivalvia	*Cucullaea*
C757B	UM		Bivalvia	*Cucullaea*
C757C2	UM		Bivalvia	*Cucullaea*
C915A.2	UM		Bivalvia	*Cucullaea*
JRB-16-0351	UW	UWBM-109960	Bivalvia	*Lahillia*
JRB-16-0729	UW	UWBM-109958	Bivalvia	*Lahillia*
JRB-16-0877	UW	UWBM-109964	Bivalvia	*Lahillia*
JRB-16-0330	UW	UWBM-109965	Bivalvia	*Lahillia*
L1134A	UM		Bivalvia	*Lahillia*
L1161B	UM		Bivalvia	*Lahillia*
L1161Sed	UM		Sediment	Sediment
L1430A1	UM		Bivalvia	*Lahillia*
L1474A1	UM		Bivalvia	*Lahillia*
L1480C	UM		Bivalvia	*Lahillia*
L1480D	UM		Bivalvia	*Lahillia*
L1516A	UM		Bivalvia	*Lahillia*
L1516B	UM		Bivalvia	*Lahillia*
L1516C	UM		Bivalvia	*Lahillia*
L1529B	UM		Bivalvia	*Lahillia*
L1529C	UM		Bivalvia	*Lahillia*
L1609	UM		Bivalvia	*Lahillia*
L477B	UM		Bivalvia	*Lahillia*
L477D	UM		Bivalvia	*Lahillia*
L757A	UM		Bivalvia	*Lahillia*
L757C	UM		Bivalvia	*Lahillia*
SI-11-466A-1	UW	UWBM-109966	Gastropoda	*Amberleya* (*Ambercyclus*? Witts et al., 2016)
SI-11-528A-1	UW	UWBM-109967	Gastropoda	*Amberleya* (*Ambercyclus*? Witts et al., 2016)
SI-11-570A-1	UW	UWBM-109968	Bivalvia	*Lahillia*
SI-11-570S-2	UW	UWBM-109969	Sediment	Sediment
SI-11-624A-2	UW	UWBM-109970	Bivalvia	*Lahillia*
SI-11-624S-1	UW	UWBM-109971	Sediment	Sediment
SI-11-722A-1	UW	UWBM-109972	Bivalvia	*Lahillia*
SI-11-722S-1	UW	UWBM-109973	Sediment	Sediment

*Institution name: UW – University of Washington, UM – University of Michigan

Data Repository Table DR2. Seymour Island age model tie points

Tie Point	Stratigraphic Height (m) Tobin et al. 2012	Stratigraphic Height (m) Zinsmeister 2001	Age (Ma)	Reference
29R-29N	924	1118	65.724	Sprain et al., 2018
KPg Boundary	865	1059	66.052	Sprain et al., 2018
30N-29R	789	983	66.311	Sprain et al., 2018
30R-30N	607	801	68.196	GTS 2012

Data Repository Table DR3. Global age model tie points

Tie Point	ODP 690 Stratigraphic Height (m) Hamilton, 1990	ODP1209 Age (Ma) Barnet et al., 2018	ODP1262 Age (Ma) Henehan et al., 2016	ODP1262 Age (Ma) Westerhold et al., 2008
29R-29N	247.55	65.608	-	64.192
KPg Boundary	247.82	66.022	66.04	65.28
30N-29R	252.58	66.407	66.398	65.625
30R-30N	-	-	-	-

Data Repository Table DR4. Trace element and $\delta^{44/40}$Ca dataset [*See Excel sheet*]

Data Repository Table DR5. ^{87}Sr/^{86}Sr dataset [*See Excel sheet*]

Data Repository Table DR6. Summary statistics of replicates

Replicate type	Average range* $\delta^{44/40}$Ca (‰)	Number of samples	Number of analyses
Sample	0.0257	10	21
Horizon	0.0383	11	32

*Average maximum minus minimum value for replicate analyses as defined in the table.

Data Repository Table DR7. Range of calcium concentration for the Late Cretaceous

Residence time τ_{Ca} (Myr)	Scale for τ_{Ca}	Reservoir size (mol)	[Ca] (mmol/kg)	Reference
0.45	1	1.44E+19	6.00E-03	Du Vivier et al., 2015
1.27	2.83	4.08E+19	1.70E-02	Horita et al., 2002
0.68	1.5	2.16E+19	9.00E-03	Lasaga et al., 1985; Wilkinson and Algeo, 1989
1.50	3.34	4.80E+19	2.00E-02	Stanley and Hardie, 1998
2.25	5	7.20E+19	3.00E-02	Hardie, 1996
3.75	8.34	1.20E+20	5.00E-02	Wallmann, 2001

Data Repository Table DR8. Flux balance model parameters

Symbol	Description	Value	Reference
F_w	Weathering input flux	3.2E+13 mol/yr	Sum input flux Du Vivier et al., 2015
δ_w	Weathering input isotope ratio	-1.12‰	Du Vivier et al., 2015
Δ_C	Carbonate Fractionation factor	-1.12‰	Du Vivier et al., 2015
δ_{SWi}	Initial isotope ratio of seawater	0.00‰	Zhu and Macdougall, 1998

Supplementary Discussion: Full description of geological setting

The López de Bertodano Formation (LBF) was deposited in the James Ross Basin during the Maastrichtian-Danian and predominantly comprises siliciclastic clays and silts with rarer sandy horizons. While the LBF has commonly been considered as deposited in an open-ocean facing shelf environment (Macellari, 1988), redox proxies have implied some degree of circulation restriction (Schoepfer et al., 2017). Carbonate concretions are common within the mudrock facies, and sandier beds often have calcareous cements. The upper 300 m of the section comprise bioturbated siltstones with occasional mappable glauconite-rich horizons capped by lags of mollusks and other fossils (Macellari, 1988; Olivero, 2012; Witts et al., 2015). Glauconite-rich horizons suggest sediment starvation and possibly record flooding surfaces formed in response to short-duration, low-amplitude sea level rises (Chafetz and Reid, 2000). Sharp boundaries above glauconitic layers may suggest shallower deposition with storm scouring. Mean sedimentation rates are estimated to be between 10 and 30 cm/kyr using dinoflagellate cyst and ammonite biostratigraphy, with comparison to magnetostratigraphy and the K-Pg boundary horizon (Witts et al., 2015). Magnetostratigraphically constrained sedimentation rates range from 10 to 20 cm/kyr (Tobin et al., 2012).

There is broad agreement on a deepening upward trend during the deposition of the LBF, but specific depth interpretations vary. Estimates of water depth for deposition of the upper LBF range from 100-200 m (Huber, 1988; Macellari, 1988); however, Crame et al. (2004) argued for deeper outer shelf conditions. The uppermost portion of the section containing samples analyzed in this study has a generally uniform sedimentology, which suggests no appreciable differences in water depth between the specimens (Crame et al., 2004). Despite a lack of sedimentological change, Macellari (1988) used paleoecological change to infer a regression roughly 50 m below the K-Pg boundary, which may instead be a biological event (Tobin, 2017).

Post-depositional alteration of the LBF appears minimal; the formation dips shallowly at 10° to the southeast, and many mollusks are preserved with nacreous aragonite that maintains iridescence, indicating that temperatures remained below 60°C (Tobin et al., 2012). The absence of any smectite-illite clay transformation and the presence of apatite fission tracks also suggests low burial temperatures (<80°C) and shallow depths (Pirrie, 1994). This evidence, combined with published data, indicates that many shells from this location are well-preserved and suitable for application to paleoclimate and paleoenvironmental reconstructions (Tobin et al., 2012; Tobin and Ward, 2015; Petersen et al., 2016; Witts et al., 2018).

Supplementary Discussion: Extended analytical methods

Elemental concentrations

Approximately 50 mg samples powdered by hand drilling or crushing chips were weighed into acid-cleaned centrifuge tubes and dissolved in ultrapure 5% HNO_3. Outgassed CO_2 was released after ~10 minutes of dissolution, when most powder had dissolved. Centrifuge tubes containing mixtures were then placed on a rocker table overnight. The mixtures were centrifuged and passed through 0.45 µm filters to obtain stock solutions. An aliquot of each stock solution was diluted to an estimated 12 ppm [Ca] in 7 mL of 5% HNO_3. Elemental concentrations were measured using a Thermo Scientific iCAP 6500 ICP-OES in the Aqueous Geochemistry Laboratory at Northwestern University. Standardization and instrument performance were checked with repeated measurements of NIST SRM 1643f.

Calcium isotope ratios ($^{44}Ca/^{40}Ca$)

Stable calcium isotope ratios ($^{44}Ca/^{40}Ca$) were measured in the Radiogenic Isotope Clean Laboratory at Northwestern University using an optimized ^{43}Ca-^{42}Ca double-spike TIMS technique (Lehn et al., 2013). Measurements were done using a Thermo-Scientific Multicollector Triton Thermal Ionization Mass Spectrometer equipped with 10^{11} Ω amplifier resistors. All procedures employed ultrapure reagents. Total procedural blanks determined by isotope dilution averaged 29 ng of Ca (n = 8), which is negligible compared to the amount of Ca processed for isotopic analysis (50 µg).

Sample aliquots containing 50 µg of Ca were weighed into Teflon vials, spiked, and equilibrated at 60 °C overnight on a hotplate. Solutions were dried at 90 °C, and the residues were dissolved in 0.5 mL of 1.55N HCl. Calcium was separated from other elements by eluting samples through Teflon columns packed with Bio-Rad AG MP-50 cation exchange resin. The purified fractions were dried, reacted with 2 drops of 35% H_2O_2 to oxidize organic compounds, reacted with 2 drops of 16N HNO_3 to convert Ca to nitrate form, and dried. The residues were dissolved in 0.4 µL of 8N HNO_3 and then split into 4 equal beads containing ~12 µg of Ca. A single bead was loaded onto outgassed, single Ta filament assemblies between thin parafilm "dams" spaced ~0.5 mm apart. The beads were dried slowly at 1.6 amps, and then 1.0 µL of 10% H_3PO_4 was added before a final dry down at 3.5 amps.

In the mass-spectrometer, a 20V ^{40}Ca ion-beam was achieved after warm-up, and $^{40}Ca/^{42}Ca$, $^{43}Ca/^{42}Ca$, and $^{43}Ca/^{44}Ca$ ratios were measured using a three-hop duty cycle having variable integration times. Amplifier biases were cancelled using amplifier rotation, and the ^{41}K beam was monitored to confirm that ^{40}K did not isobarically interfere with ^{40}Ca ($^{40}K/^{41}K$ = 0.00174). Datasets comprising 120 scans were reduced using an iterative procedure. All runs were evaluated to ensure a steady or increasing ^{40}Ca beam, an increasing raw $^{42}Ca/^{40}Ca$ fractionation pattern, and the absence of filament reservoir effects, which appear as "reverse-fractionation" in uncorrected ratios or residual trends in fractionation-corrected ratios. Changes in collector cup efficiency were monitored and accounted for by analyzing at least 6 Ocean Scientific International Ltd. (OSIL) seawater (SW) standards and 2 NIST 915b standards every 30 samples. All results are reported in delta notation relative to SW. The internal precision of the sample runs ranged from ±0.016‰ to ±0.027‰ (2SEM). During the period of study, repeated analyses of OSIL SW and NIST 915b yielded mean $\delta^{44/40}Ca$ values of 0.00‰ ± 0.009‰ (2SEM, n = 37) and NIST -1.13 ± 0.016‰ (2SEM, n = 10). These results correspond to a short-term,

external reproducibility of ±0.05‰ (2SD), which is the uncertainty adopted for the present study. As described in the main text, replicates of samples were better than ±0.05‰.

Radiogenic strontium isotope ratios ($^{87}Sr/^{86}Sr$)

Strontium isotope ratios ($^{87}Sr/^{86}Sr$) were also measured in the Radiogenic Isotope Clean Laboratory at Northwestern University, following the TIMS procedure outlined in Andrews et al. (2016). Sample aliquots containing 100 ng of Sr were dried in Teflon vials, and the residues were dissolved in 8 M HNO_3. Strontium was separated from matrix elements by eluting samples through inverted pipet tips packed with Eichrom Sr-Spec resin. The purified fractions were dried, and the residues were dissolved in 1.5 µL 3 N HNO_3. The aliquots were loaded onto outgassed, single Re filament assemblies, together with 1 µL of a $TaCl_5$ activator solution, and dried at 1.0 amps before heating to ~2.2 amps. In the mass-spectrometer, an 8V ^{88}Sr ion-beam was achieved before collecting data in multi-dynamic mode for 120 duty cycles having a 4 s integration time. Measurements were made with amplifier rotation. The ^{85}Rb beam was monitored to ensure that ^{87}Rb did not isobarically interfere with ^{87}Sr ($^{87}Rb/^{85}Rb = 0.3856$). Instrumental mass fractionation was corrected by normalizing $^{86}Sr/^{88}Sr$ ratios to 0.1194 using an exponential law. During the period of study, measurements of NBS 987 yielded an $^{87}Sr/^{86}Sr$ of 0.710252 ± 0.000008 (2SD, n =5).

Supplementary Discussion: Description of age model and correlation

Seymour Island Age model:

The age model for many of the samples builds on the stratigraphic framework outlined by Zinsmeister (2001), where plane projection was used to place georeferenced samples distributed across the island onto a unified stratigraphic section. Several samples analyzed in this study were collected within a measured stratigraphic section (Tobin et al., 2012). Placement of samples from the Tobin et al. (2012) framework into the Zinsmeister (2001) framework was done by adding 194 m to the stratigraphic height. This same stratigraphic framework has been used for previous geochemical studies (Petersen et al., 2016) and the analysis of the K-Pg extinction (Wang and Marshall, 2004; Tobin, 2017). Stratigraphic thicknesses for Molluscan Units, as defined by Macellari (1988), are within ~4 m between the Tobin et al. (2012) and Zinsmeister (2001) frameworks (Petersen et al., 2016). Analyses of $\delta^{18}O$ and $\delta^{13}C$ from samples in both frameworks are comparable (Tobin et al., 2012). Given fixed sedimentation rates, ±4 m uncertainty is equivalent to age uncertainties of ~13 to ~40 kyr. It should also be noted that the relative ordering of samples is robust relative to the K-Pg horizon due to significant lithological changes and the high sedimentation rates in the location.

Numerical ages for the section are derived assuming constant rates of sediment accumulation between chron reversals and the K-Pg boundary. Magnetostrigraphic reversals (C30R-C30N-C29R-C29N) are documented in the López de Bertodano Formation (Tobin et al., 2012). The age of one sample (JRB-16-0877) from 11 m above the base of C29N is extrapolated assuming the same sedimentation rate. Ages used for these reversals are from Sprain et al. (2018) and Gradstein et al. (2012). The age used for the K-Pg boundary is 66.052 Ma (Sprain et al., 2018). Correlation to other globally distributed datasets are outlined in the following paragraphs, and Table DR2 provides a complete list of ages used for the age model construction.

Correlation to ODP 690:

Data from ODP 690 are correlated to Seymour Island using chron reversals and the K-Pg boundary. The positions of chron reversals are from Hamilton (1990). Data on carbonate weight % are from several sources (O'Connell, 1990; Ehrendorfer, 1993). Some bioturbation near the K-Pg boundary may have produced a pre-impact decrease in carbonate weight percent due to moving carbonate up and non-carbonates lower in the core (Henehan et al., 2016), but perhaps the decrease is real and related to an increase in Deccan volcanism just before the K-Pg boundary (Ehrendorfer, 1993; Westerhold et al., 2011; Henehan et al., 2016; Dameron et al., 2017; Schoene et al., 2019; Sprain et al., 2019). For the purposes of the null hypothesis model based on flux imbalances (see below), the impact of this bioturbation is minimal and only matters slightly for low seawater calcium concentrations.

Correlation to ODP 1262:

Data from ODP 1262, as presented in Barnet et al. (2018), were correlated to the Seymour Island section by adjusting all data based on a slightly different K-Pg boundary age of 66.052 Ma (Sprain et al., 2018) rather than the astronomically tuned age of 66.02 Ma (Dinarès-Turell et al., 2014) used by Barnet et al. (2018). We also tie the C30N-C29R and C29R-C29N reversal ages to that from Sprain et al. (2018) and linearly scale astronomically tuned numeric ages between the two. Similar correlations to this dataset have been done recently by other authors (Schoene et al., 2019; Sprain et al., 2019). It should also be noted that the sedimentation rates differ greatly between 1 – 2 cm/kyr at ODP sites and 10 – 30 cm/kyr at Seymour Island.

Correlation to ODP 1209:

Data from ODP 1209, as presented in Westerhold et al. (2011) and Henehan et al. (2016), are correlated to our section by adjusting the ages of the K-Pg, C30N-C29R, and C29R-C29N to updated ages from Sprain et al. (2018) and scaling their published ages between these tie points.

Correlation to Deccan Traps flow volumes:

Deccan Traps flow volumes are from Richards et al. (2015), and durations of flows are from Sprain et al. (2019). Eruption rate estimates are from U-Pb dating of zircons done by Schoene et al., (2019) and are scaled linearly between the K-Pg and C30N-C29R. Correlation between these records is done using the same chron reversals and the K-Pg.

Uncertainty in the age model:

Correlation of data from Seymour Island to other records hinges on the assumption of continuous steady rate sedimentation in this location and other locations, if solely tied together using chron reversals and the K-Pg boundary. Future work at Seymour Island, including astronomically tuned age models, will help determine the validity of this assumption.

Supplementary Discussion: Description of illustrative box model

A simple numerical model of the marine Ca isotope cycle is used to constrain drivers of $\delta^{44/40}$Ca variation, specifically imbalances between primary input and output fluxes (Fig. 4, Fig. DR4). The model presents a simple null hypothesis for $\delta^{44/40}$Ca variation caused by changes in the 'weathering flux' relative to the 'carbonate flux.' Flux imbalance is hypothesized to be one of the major drivers of $\delta^{44/40}$Ca evolution through Earth history (DePaolo, 2004; Fantle and

DePaolo, 2005; Fantle, 2010; Fantle and Tipper, 2014; Tipper et al., 2016). Although more complex modeling—coupling to seawater carbonate chemistry and pCO_2 weathering feedbacks, for example—can be done for the marine $\delta^{44/40}$Ca system, difficulties persist in reproducing $\delta^{44/40}$Ca excursions measured in carbonates because isotope fractionation mechanisms remain incompletely understood (Komar and Zeebe, 2016; Jost et al., 2016; Silva-Tamayo et al., 2018). Relative uniformity of the $^{87}Sr/^{86}Sr$ record (Fig. 3) suggests that the weathering flux did not substantially change over the sampled interval, so in the subsequent forward model, we assume a constant weathering flux and a variable carbonate burial flux. This model is parameterized using the same fluxes and Ca isotope compositions as Du Vivier et al. (2015), but higher [Ca] values and longer residence times. This model is intended to explain horizon-to-horizon variations through changes in the $\delta^{44/40}$Ca composition of seawater, but not reproduce the absolute $\delta^{44/40}$Ca values of mollusk shell due to unknown controls on biogenic fractionation (see extended discussion below).

The forward model for the $\delta^{44/40}$Ca of seawater based on flux imbalances is done assuming equality of the weathering input flux (F_w) and carbonate export flux (F_{carb}) at 66.5 Ma. F_{carb} is then scaled by changes in carbonate weight percent (wt_{carb}) from this point in time. For example, if wt_{carb} is reduced by 50% from the initial value (e.g., 90% to 45%), then F_{carb} is reduced by 50%. In this modeling, the initial mass of calcium in the ocean is run at the limits of estimated ranges for Late Cretaceous seawater (~10 to 50 mmol/kg, Lasaga et al., 1985; Wallmann, 2001). To create an initial steady state with a fixed F_w across the range of masses modeled here, initial F_{carb} must remain constant. In this model, F_{carb} is equivalent to the moles of Ca in the ocean (N_{Ca}) divided by the residence time of Ca (τ_{Ca}), so to maintain an initial steady state any adjustment to N_{Ca} also requires an adjustment to τ_{Ca}. We scale both by multiplying by a constant scaling factor to allow a fixed F_w for all model runs (Table DR 7). The model equations are:

1) $$\frac{dN_{Ca}}{dt} = Fw - \frac{wt_{carb_t}}{wt_{carb_i}} * \frac{N_{Ca_t}}{\tau_{Ca}}$$

2) $$\frac{d(N_{Ca}\delta_{SW})}{dt} = Fw * \delta_W - (\delta_{SW} + \Delta_C) * \frac{wt_{carb_t}}{wt_{carb_i}} * \frac{N_{Ca_t}}{\tau_{Ca}}$$

where fixed variables were set using values in Table DR8. The carbonate weight percent that varies F_{carb} in the model is a loess-smoothed and interpolated record of ODP site 690 combining several data sources (O'Connell, 1990; Ehrendorfer, 1993), which is correlated into the Seymour Island timescale as outlined above. With this method, F_{carb} reduction at the K-Pg boundary is likely overestimated because indications of carbonate preservation (e.g., coarse fraction, unbroken planktic foraminifera) increase in multiple cores immediately after the boundary (Henehan et al., 2016). This occurs because wt_{carb} may have decreased in any single core, while another area could have preserved carbonate due to increased saturation of the whole ocean (Henehan et al., 2016; Luo et al., 2016; Boudreau et al., 2018). In other words, although wt_{carb} goes down in one location, alkalinity buildup in the global ocean may enhance carbonate preservation in others. Additionally, changes in wt_{carb} are sensitive to carbonate production, including biological productivity, saturation state at the seafloor, riverine runoff, and the proportion of foraminifera to coccolithophores (Henehan et al., 2016). Because of these complex

controls, wt_{carb} is likely a better flux estimator than a highly sensitive saturation state proxy (Henehan et al., 2016).

To reproduce the relative mollusk $\delta^{44/40}$Ca pattern by maintaining a fixed fractionation factor and allowing $\delta^{44/40}Ca_{SW}$ to vary due to flux imbalances, substantial (4x or more) and high frequency (<200 kyr) shifts in weathering and carbonate fluxes are required. Although weathering rates may have increased somewhat through the interval (Martin and Macdougall, 1991; McArthur et al., 1998; Dessert et al., 2001; Tobin et al., 2017), it seems unlikely that either weathering or carbonate fluxes can vary by such large magnitudes over brief time spans. Moreover, the absence of variation in the measured $^{87}Sr/^{86}Sr$ record precludes substantial changes in weathering.

Reduced aragonite export is expected during OA (Orr et al., 2005), but decreases in the proportion of aragonite-to-calcite burial drive $\delta^{44/40}Ca_{SW}$ in the opposite direction relative to the observed record. Moreover, OA is expected to reduce fractionation for all carbonate minerals (Tang et al., 2008; Nielsen et al., 2012), which causes similar discrepancies between measured and modeled data.

Supplementary Discussion: Discussion of calcium isotope fractionation and biomineralization

Mollusk carbonate offers a valuable geochemical archive because of the abundant methods available to screen shells for diagenetic alteration (Cochran et al., 2010; Witts et al., 2018). Nonetheless, biological control of Ca isotope fractionation (Gussone and Heuser, 2016) and averaging timescales of growth and shell accumulation (Kidwell, 2002; Judd et al., 2018; Linzmeier et al., 2018) add complexity to interpreting data derived from these materials.

Data presented in this paper span several temporal scales. First, the analysis of each shell averages multiple years of growth (Petersen et al., 2016). This masks any seasonal variability that might be coupled to temperature (Immenhauser et al., 2005; Steuber and Buhl, 2006; Hippler et al., 2013) or seasonal changes in the carbonate chemistry of local seawater (Kelly and Hofmann, 2013; Waldbusser and Salisbury, 2014). Second, replicate shells from the same or closely spaced stratigraphic levels demonstrate $\delta^{44/40}$Ca variability on the timescales of hundreds to thousands of years necessary for shell bed accumulations (Kidwell, 2002). Similarity between shells from the same horizons suggest environmental conditions that control $\delta^{44/40}$Ca persist over shell accumulation timescales. Third, level-to-level variability through the section represents mean changes in environmental parameters that drive $\delta^{44/40}$Ca across timescales of tens of thousands of years, as derived from the linear sedimentation age model.

More study of modern mollusks is needed to address Ca isotope fractionation by these organisms but placing our data in context of globally distributed proxies suggests a CO_2-linked driver. It is beyond the present dataset to determine the exact mechanism of fractionation in these mollusks, but our findings suggest investigations of covariation between carbonate saturation state and $\delta^{44/40}$Ca are merited. Samples from natural environments with different pCO_2 and therefore carbonate saturation states may provide the best analog to changes experienced by organisms on intergenerational timescales as the K-Pg mollusks experienced. Existing datasets may be reinterpreted in this context given poor fit to temperatures (Hippler et al., 2013). Given covariation with sedimentary indicators of saturation, fractionation may mimic responses seen in abiotic precipitation experiments, at least in sign (Tang et al., 2008; Nielsen et al., 2012). The

mechanism of fractionation may lie in calcium transport into the extrapallial fluid (EPF). Precipitation of shell is isolated from seawater in the EPF between the shell and mantle. Mollusks regulate the pH and saturation state of EPF (Heinemann et al., 2012). Intracellular calcium channels move most of the calcium into the EPF, and they enable high, selective diffusive fluxes which are controlled by biomineralization rates (Carré et al., 2006). Other pathways, such as passive, non-selective intercellular Ca transport and active enzymatic (Ca2+-ATPase and carbonic anhydrase) pumping, may also fractionate calcium isotopes (Carré et al., 2006).

Supplementary References:

Barnet, J.S.K., Littler, K., Kroon, D., Leng, M.J., Westerhold, T., Röhl, U., and Zachos, J.C., 2018, A new high-resolution chronology for the late Maastrichtian warming event: Establishing robust temporal links with the onset of Deccan volcanism: Geology, v. 46, p. 147–150, doi:10.1130/G39771.1.

Berner, E.K., and Berner, R.A., 2012, Global Environment: Water, Air, and Geochemical Cycles - Second Edition: Princeton University Press, 461 p.

Blättler, C.L., Henderson, G.M., and Jenkyns, H.C., 2012, Explaining the Phanerozoic Ca isotope history of seawater: Geology, v. 40, p. 843–846, doi:10.1130/G33191.1.

Boudreau, B.P., Middelburg, J.J., and Luo, Y., 2018, The role of calcification in carbonate compensation: Nature Geoscience, v. 11, p. 894, doi:10.1038/s41561-018-0259-5.

Carré, M., Bentaleb, I., Bruguier, O., Ordinola, E., Barrett, N.T., and Fontugne, M., 2006, Calcification rate influence on trace element concentrations in aragonitic bivalve shells: Evidences and mechanisms: Geochimica et Cosmochimica Acta, v. 70, p. 4906–4920, doi:10.1016/j.gca.2006.07.019.

Chafetz, H.S., and Reid, A., 2000, Syndepositional shallow-water precipitation of glauconitic minerals: Sedimentary Geology, v. 136, p. 29–42, doi:10.1016/S0037-0738(00)00082-8.

Cochran, J.K., Kallenberg, K., Landman, N.H., Harries, P.J., Weinreb, D., Turekian, K.K., Beck, A.J., and Cobban, W.A., 2010, Effect of diagenesis on the Sr, O, and C isotope composition of Late Cretaceous mollusks from the Western Interior Seaway of North America: American Journal of Science, v. 310, p. 69–88, doi:10.2475/02.2010.01.

Crame, J.A., Francis, J.E., Cantrill, D.J., and Pirrie, D., 2004, Maastrichtian stratigraphy of Antarctica: Cretaceous Research, v. 25, p. 411–423, doi:10.1016/j.cretres.2004.02.002.

Dameron, S.N., Leckie, R.M., Clark, K., MacLeod, K.G., Thomas, D.J., and Lees, J.A., 2017, Extinction, dissolution, and possible ocean acidification prior to the Cretaceous/Paleogene (K/Pg) boundary in the tropical Pacific: Palaeogeography, Palaeoclimatology, Palaeoecology, v. 485, p. 433–454, doi:10.1016/j.palaeo.2017.06.032.

DePaolo, D.J., 2004, Calcium isotopic variations produced by biological, kinetic, radiogenic and nucleosynthetic processes: Reviews in Mineralogy and Geochemistry, v. 55, p. 255–288, doi:10.2138/gsrmg.55.1.255.

Dessert, C., Dupré, B., François, L.M., Schott, J., Gaillardet, J., Chakrapani, G., and Bajpai, S., 2001, Erosion of Deccan Traps determined by river geochemistry: Impact on the global climate and the $^{87}Sr/^{86}Sr$ ratio of seawater: Earth and Planetary Science Letters, v. 188, p. 459–474, doi:10.1016/S0012-821X(01)00317-X.

Dinarès-Turell, J., Westerhold, T., Pujalte, V., Röhl, U., and Kroon, D., 2014, Astronomical calibration of the Danian stage (Early Paleocene) revisited: Settling chronologies of sedimentary records across the Atlantic and Pacific Oceans: Earth and Planetary Science Letters, v. 405, p. 119–131, doi:10.1016/j.epsl.2014.08.027.

Du Vivier, A.D.C., Jacobson, A.D., Lehn, G.O., Selby, D., Hurtgen, M.T., and Sageman, B.B., 2015, Ca isotope stratigraphy across the Cenomanian–Turonian OAE 2: Links between volcanism, seawater geochemistry, and the carbonate fractionation factor: Earth and Planetary Science Letters, v. 416, p. 121–131, doi:10.1016/j.epsl.2015.02.001.

Ehrendorfer, T.W., 1993, Late Cretaceous (Maestrichtian) calcareous nannoplankton biogeography with emphasis on events immediately preceding the Cretaceous/Paleocene boundary [Ph.D.]: Massachusetts Institute of Technology.

Fabry, V., McClintock, J., Mathis, J., and Grebmeier, J., 2009, Ocean Acidification at High Latitudes: The Bellwether: Oceanography, v. 22, p. 160–171, doi:10.5670/oceanog.2009.105.

Fantle, M.S., 2010, Evaluating the Ca isotope proxy: American Journal of Science, v. 310, p. 194–230, doi:10.2475/03.2010.03.

Fantle, M.S., and DePaolo, D.J., 2005, Variations in the marine Ca cycle over the past 20 million years: Earth and Planetary Science Letters, v. 237, p. 102–117, doi:10.1016/j.epsl.2005.06.024.

Fantle, M.S., and Tipper, E.T., 2014, Calcium isotopes in the global biogeochemical Ca cycle: Implications for development of a Ca isotope proxy: Earth-Science Reviews, v. 129, p. 148–177, doi:10.1016/j.earscirev.2013.10.004.

Gradstein, F.M., Ogg, J.G., Schmitz, M., and Ogg, G., 2012, The Geologic Time Scale 2012: Elsevier, 1175 p.

Gussone, N., and Heuser, A., 2016, Biominerals and Biomaterial, *in* Calcium Stable Isotope Geochemistry, Berlin, Heidelberg, Springer Berlin Heidelberg, p. 111–144, doi:10.1007/978-3-540-68953-9_4.

Hamilton, N., 1990, Mesozoic magnetostratigraphy of Maud Rise, Antarctica, *in* Proceedings of the Ocean Drilling Program: Scientific Results, College Station, TX, Ocean Drilling Program, v. 113, p. 255–260.

Hardie, L.A., 1996, Secular variation in seawater chemistry: An explanation for the coupled secular variation in the mineralogies of marine limestones and potash evaporites over the past 600 m.y.: Geology, v. 24, p. 279–283, doi:10.1130/0091-7613(1996)024<0279:SVISCA>2.3.CO;2.

Heinemann, A., Fietzke, J., Melzner, F., Böhm, F., Thomsen, J., Garbe-Schönberg, D., and Eisenhauer, A., 2012, Conditions of *Mytilus edulis* extracellular body fluids and shell composition in a pH-treatment experiment: Acid-base status, trace elements and $\delta^{11}B$: Geochemistry, Geophysics, Geosystems, v. 13, p. Q01005, doi:10.1029/2011GC003790.

Henehan, M.J., Hull, P.M., Penman, D.E., Rae, J.W.B., and Schmidt, D.N., 2016, Biogeochemical significance of pelagic ecosystem function: An end-Cretaceous case study: Phil. Trans. R. Soc. B, v. 371, p. 20150510, doi:10.1098/rstb.2015.0510.

Hippler, D., Witbaard, R., van Aken, H.M., Buhl, D., and Immenhauser, A., 2013, Exploring the calcium isotope signature of *Arctica islandica* as an environmental proxy using laboratory- and field-cultured specimens: Palaeogeography, Palaeoclimatology, Palaeoecology, v. 373, p. 75–87, doi:10.1016/j.palaeo.2011.11.015.

Horita, J., Zimmermann, H., and Holland, H.D., 2002, Chemical evolution of seawater during the Phanerozoic: Implications from the record of marine evaporites: Geochimica et Cosmochimica Acta, v. 66, p. 3733–3756, doi:10.1016/S0016-7037(01)00884-5.

Huber, B.T., 1988, Upper Campanian-Paleocene foraminifera from the James Ross Island region, Antarctic Peninsula, *in* Geological Society of America Memoirs, Geological Society of America, v. 169, p. 163–252, doi:10.1130/MEM169-p163.

Immenhauser, A., Nägler, T.F., Steuber, T., and Hippler, D., 2005, A critical assessment of mollusk $^{18}O/^{16}O$, Mg/Ca, and $^{44}Ca/^{40}Ca$ ratios as proxies for Cretaceous seawater temperature seasonality: Palaeogeography, Palaeoclimatology, Palaeoecology, v. 215, p. 221–237, doi:10.1016/j.palaeo.2004.09.005.

Jost, A.B., Bachan, A., van de Schootbrugge, B., Brawn, S.T., DePaolo, D.J., and Payne, J.L., 2016, Additive effects of acidification and mineralogy on calcium isotopes in Triassic/Jurassic boundary limestones: Geochemistry, Geophysics, Geosystems, v. 18, p. 113–124, doi:10.1002/2016GC006724.

Judd, E.J., Wilkinson, B.H., and Ivany, L.C., 2018, The life and time of clams: Derivation of intra-annual growth rates from high-resolution oxygen isotope profiles: Palaeogeography, Palaeoclimatology, Palaeoecology, v. 490, p. 70–83, doi:10.1016/j.palaeo.2017.09.034.

Kelly, M.W., and Hofmann, G.E., 2013, Adaptation and the physiology of ocean acidification: Functional Ecology, v. 27, p. 980–990, doi:10.1111/j.1365-2435.2012.02061.x.

Kidwell, S.M., 2002, Time-averaged molluscan death assemblages: Palimpsests of richness, snapshots of abundance: Geology, v. 30, p. 803–806, doi:10.1130/0091-7613(2002)030<0803:TAMDAP>2.0.CO;2.

Komar, N., and Zeebe, R.E., 2016, Calcium and calcium isotope changes during carbon cycle perturbations at the end-Permian: Paleoceanography, v. 31, p. 115–130, doi:10.1002/2015PA002834.

Lasaga, A.C., Berner, R.A., Garrels, R.M., Sundquist, E.T., and Broecker, W.S., 1985, An improved geochemical model of atmospheric CO_2 fluctuations Over the past 100 million years, *in* The Carbon Cycle and Atmospheric CO_2: Natural Variations Archean to Present, American Geophysical Union (AGU), Geophysics Monograph, v. 32, p. 397–411, doi:10.1029/GM032p0397.

Lehn, G.O., Jacobson, A.D., and Holmden, C., 2013, Precise analysis of Ca isotope ratios ($\delta^{44/40}$Ca) using an optimized ^{43}Ca–^{42}Ca double-spike MC-TIMS method: International Journal of Mass Spectrometry, v. 351, p. 69–75, doi:10.1016/j.ijms.2013.06.013.

Linzmeier, B.J., Landman, N.H., Peters, S.E., Kozdon, R., Kitajima, K., and Valley, J.W., 2018, Ion microprobe–measured stable isotope evidence for ammonite habitat and life mode during early ontogeny: Paleobiology, v. 44, p. 684–708, doi:10.1017/pab.2018.21.

Luo, Y., Boudreau, B.P., Dickens, G.R., Sluijs, A., and Middelburg, J.J., 2016, An alternative model for $CaCO_3$ over-shooting during the PETM: Biological carbonate compensation: Earth and Planetary Science Letters, v. 453, p. 223–233, doi:10.1016/j.epsl.2016.08.012.

Macellari, C.E., 1988, Stratigraphy, sedimentology, and paleoecology of Upper Cretaceous/Paleocene shelf-deltaic sediments of Seymour Island, *in* Geological Society of America Memoirs, Geological Society of America, v. 169, p. 25–54, doi:10.1130/MEM169-p25.

Martin, E.E., and Macdougall, J.D., 1991, Seawater Sr isotopes at the Cretaceous/Tertiary boundary: Earth and Planetary Science Letters, v. 104, p. 166–180, doi:10.1016/0012-821X(91)90202-S.

McArthur, J.M., Thirlwall, M.F., Engkilde, M., Zinsmeister, W.J., and Howarth, R.J., 1998, Strontium isotope profiles across K/T boundary sequences in Denmark and Antarctica: Earth and Planetary Science Letters, v. 160, p. 179–192, doi:10.1016/S0012-821X(98)00058-2.

Nielsen, L.C., DePaolo, D.J., and De Yoreo, J.J., 2012, Self-consistent ion-by-ion growth model for kinetic isotopic fractionation during calcite precipitation: Geochimica et Cosmochimica Acta, v. 86, p. 166–181, doi:10.1016/j.gca.2012.02.009.

O'Connell, S.B., 1990, Variations in Upper Cretaceous and Cenozoic calcium carbonate percentages, Maud Rise, Weddell Sea, Antarctica, *in* Proceedings of the Ocean Drilling Program Science Results, College Station, TX, Ocean Drilling Program, v. 113, p. 971–984.

Olivero, E.B., 2012, Sedimentary cycles, ammonite diversity and palaeoenvironmental changes in the Upper Cretaceous Marambio Group, Antarctica: Cretaceous Research, v. 34, p. 348–366, doi:10.1016/j.cretres.2011.11.015.

Orr, J.C. et al., 2005, Anthropogenic ocean acidification over the twenty-first century and its impact on calcifying organisms: Nature, v. 437, p. 681, doi:10.1038/nature04095.

Petersen, S.V., Dutton, A., and Lohmann, K.C., 2016, End-Cretaceous extinction in Antarctica linked to both Deccan volcanism and meteorite impact via climate change: Nature Communications, v. 7, p. 12079, doi:10.1038/ncomms12079.

Pirrie, D., 1994, Petrography and provenance of the Marambio Group, Vega Island, Antarctica: Antarctic Science, v. 6, doi:10.1017/S0954102094000775.

Richards, M.A., Alvarez, W., Self, S., Karlstrom, L., Renne, P.R., Manga, M., Sprain, C.J., Smit, J., Vanderkluysen, L., and Gibson, S.A., 2015, Triggering of the largest Deccan eruptions by the Chicxulub impact: GSA Bulletin, v. 127, p. 1507–1520, doi:10.1130/B31167.1.

Schoene, B., Eddy, M.P., Samperton, K.M., Keller, C.B., Keller, G., Adatte, T., and Khadri, S.F.R., 2019, U-Pb constraints on pulsed eruption of the Deccan Traps across the end-Cretaceous mass extinction: Science, v. 363, p. 862–866, doi:10.1126/science.aau2422.

Schoepfer, S.D., Tobin, T.S., Witts, J.D., and Newton, R.J., 2017, Intermittent euxinia in the high-latitude James Ross Basin during the latest Cretaceous and earliest Paleocene: Palaeogeography, Palaeoclimatology, Palaeoecology, v. 477, p. 40–54, doi:10.1016/j.palaeo.2017.04.013.

Silva-Tamayo, J.C. et al., 2018, Global perturbation of the marine calcium cycle during the Permian-Triassic transition: GSA Bulletin, v. 130, p. 1323–1338, doi:10.1130/B31818.1.

Sprain, C.J., Renne, P.R., Clemens, W.A., and Wilson, G.P., 2018, Calibration of chron C29r: New high-precision geochronologic and paleomagnetic constraints from the Hell Creek region, Montana: GSA Bulletin, v. 130, p. 1615–1644, doi:10.1130/B31890.1.

Sprain, C.J., Renne, P.R., Vanderkluysen, L., Pande, K., Self, S., and Mittal, T., 2019, The eruptive tempo of Deccan volcanism in relation to the Cretaceous-Paleogene boundary: Science, v. 363, p. 866–870, doi:10.1126/science.aav1446.

Stanley, S.M., and Hardie, L.A., 1998, Secular oscillations in the carbonate mineralogy of reef-building and sediment-producing organisms driven by tectonically forced shifts in seawater chemistry: Palaeogeography, Palaeoclimatology, Palaeoecology, v. 144, p. 3–19, doi:10.1016/S0031-0182(98)00109-6.

Steuber, T., and Buhl, D., 2006, Calcium-isotope fractionation in selected modern and ancient marine carbonates: Geochimica et Cosmochimica Acta, v. 70, p. 5507–5521, doi:10.1016/j.gca.2006.08.028.

Tang, J., Dietzel, M., Böhm, F., Köhler, S.J., and Eisenhauer, A., 2008, Sr^{2+}/Ca^{2+} and $^{44}Ca/^{40}Ca$ fractionation during inorganic calcite formation: II. Ca isotopes: Geochimica et Cosmochimica Acta, v. 72, p. 3733–3745, doi:10.1016/j.gca.2008.05.033.

Tipper, E.T., Schmitt, A.-D., and Gussone, N., 2016, Global Ca Cycles: Coupling of Continental and Oceanic Processes, *in* Calcium Stable Isotope Geochemistry, Berlin, Heidelberg, Springer Berlin Heidelberg, p. 173–222, doi:10.1007/978-3-540-68953-9_6.

Tobin, T.S., 2017, Recognition of a likely two phased extinction at the K-Pg boundary in Antarctica: Scientific Reports, v. 7, p. 16317, doi:10.1038/s41598-017-16515-x.

Tobin, T.S., Bitz, C.M., and Archer, D., 2017, Modeling climatic effects of carbon dioxide emissions from Deccan Traps volcanic eruptions around the Cretaceous–Paleogene boundary: Palaeogeography, Palaeoclimatology, Palaeoecology, v. 478, p. 139–148, doi:10.1016/j.palaeo.2016.05.028.

Tobin, T.S., and Ward, P.D., 2015, Carbon isotope ($\delta^{13}C$) differences between Late Cretaceous ammonites and benthic mollusks from Antarctica: Palaeogeography, Palaeoclimatology, Palaeoecology, v. 428, p. 50–57, doi:10.1016/j.palaeo.2015.03.034.

Tobin, T.S., Ward, P.D., Steig, E.J., Olivero, E.B., Hilburn, I.A., Mitchell, R.N., Diamond, M.R., Raub, T.D., and Kirschvink, J.L., 2012, Extinction patterns, $\delta^{18}O$ trends, and magnetostratigraphy from a southern high-latitude Cretaceous–Paleogene section: Links with Deccan volcanism: Palaeogeography, Palaeoclimatology, Palaeoecology, v. 350–352, p. 180–188, doi:10.1016/j.palaeo.2012.06.029.

Waldbusser, G.G., and Salisbury, J.E., 2014, Ocean acidification in the Coastal Zone from an organism's perspective: Multiple system parameters, frequency domains, and habitats: Annual Review of Marine Science, v. 6, p. 221–247, doi:10.1146/annurev-marine-121211-172238.

Wallmann, K., 2001, Controls on the Cretaceous and Cenozoic evolution of seawater composition, atmospheric CO_2 and climate: Geochimica et Cosmochimica Acta, v. 65, p. 3005–3025, doi:10.1016/S0016-7037(01)00638-X.

Wang, S.C., and Marshall, C.R., 2004, Improved Confidence Intervals for Estimating the Position of a Mass Extinction Boundary: Paleobiology, v. 30, p. 5–18.

Westerhold, T., Röhl, U., Donner, B., McCarren, H.K., and Zachos, J.C., 2011, A complete high-resolution Paleocene benthic stable isotope record for the central Pacific (ODP Site 1209): Paleoceanography, v. 26, doi:10.1029/2010PA002092.

Wilkinson, B.H., and Algeo, T.J., 1989, Sedimentary carbonate record of calcium-magnesium cycling: American Journal of Science, v. 289, p. 1158–1194, doi:10.2475/ajs.289.10.1158.

Witts, J.D., Bowman, V.C., Wignall, P.B., Alistair Crame, J., Francis, J.E., and Newton, R.J., 2015, Evolution and extinction of Maastrichtian (Late Cretaceous) cephalopods from the López de Bertodano Formation, Seymour Island, Antarctica: Palaeogeography, Palaeoclimatology, Palaeoecology, v. 418, p. 193–212, doi:10.1016/j.palaeo.2014.11.002.

Witts, J.D., Newton, R.J., Mills, B.J.W., Wignall, P.B., Bottrell, S.H., Hall, J.L.O., Francis, J.E., and Alistair Crame, J., 2018, The impact of the Cretaceous–Paleogene (K–Pg) mass extinction event on the global sulfur cycle: Evidence from Seymour Island, Antarctica: Geochimica et Cosmochimica Acta, v. 230, p. 17–45, doi:10.1016/j.gca.2018.02.037.

Zhu, P., and Macdougall, J.D., 1998, Calcium isotopes in the marine environment and the oceanic calcium cycle: Geochimica et Cosmochimica Acta, v. 62, p. 1691–1698, doi:10.1016/S0016-7037(98)00110-0.

Zinsmeister, W.J., 2001, Late Maastrichtian Short-term Biotic Events on Seymour Island, Antarctic Peninsula: The Journal of Geology, v. 109, p. 213–229, doi:10.1086/319239.